Delivering Nanoparticles to Lungs while Avoiding Liver and Spleen through Adsorption on Red Blood Cells

Aaron C. Anselmo,[†] Vivek Gupta,[†,§] Blaine J. Zern,[‡] Daniel Pan,[‡] Michael Zakrewsky,[†] Vladimir Muzykantov,[‡] and Samir Mitragotri[†,*]

[†]Department of Chemical Engineering and Center for Bioengineering University of California, Santa Barbara, California 93106, United States and [‡]Department of Pharmacology and Center for Translational Targeted Therapeutics and Nanomedicine, Perelman School of Medicine, University of Pennsylvania, Philadelphia, Pennsylvania 19104, United States. [§]Present Address: School of Pharmacy, Keck Graduate Institute, 535 Watson Drive, Claremont, California 91711.

ABSTRACT Nanoparticulate drug delivery systems are one of the most widely investigated approaches for developing novel therapies for a variety of diseases. However, rapid clearance and poor targeting limit their clinical utility. Here, we describe an approach to harness the flexibility, circulation, and vascular mobility of red blood cells (RBCs) to simultaneously overcome these limitations (cellular hitchhiking). A noncovalent attachment of nanoparticles to RBCs simultaneously increases their level in blood over a 24 h period and allows transient accumulation in the lungs, while reducing their uptake by liver and spleen. RBC-adsorbed nanoparticles exhibited ~3-fold increase in blood persistence and ~7-fold higher accumulation in lungs. RBC-adsorbed nanoparticles improved lung/liver and lung/spleen nanoparticle accumulation by over 15-fold and 10-fold, respectively. Accumulation in lungs is attributed to mechanical transfer of particles from the RBC surface to lung endothelium. Independent tracing of both nanoparticles and RBCs *in vivo* confirmed that RBCs themselves do not accumulate in lungs. Attachment of anti-ICAM-1 antibody to the exposed surface of NPs that were attached to RBCs led to further increase in lung targeting and retention over 24 h. Cellular hitchhiking onto RBCs provides a new platform for improving the blood pharmacokinetics and vascular delivery of nanoparticles while simultaneously avoiding uptake by liver and spleen, thus opening the door for new applications.

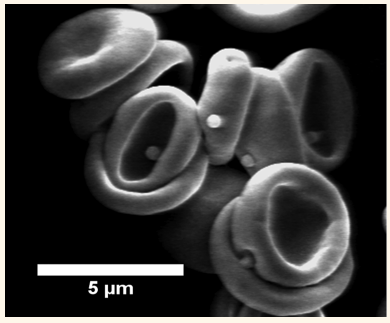

KEYWORDS: hitchhiking · cell-mediated drug delivery · nanomedicine · nanotechnology

Nanoparticles (NPs) are actively explored for encapsulation and targeted delivery of drugs for improving the current treatment strategies for cancer and other diseases.[1−3] Several preclinical studies have demonstrated the use of nanoparticles for targeting various cancers including breast, prostate, and lung.[3−7] Some of these strategies have also advanced to clinical studies and have yielded promising early results.[8−11] Encapsulation in nanoparticles provides distinct advantages over free drugs including targeting and sustained release.[12,13] Nanoparticles, however, suffer from the limitation of rapid clearance by the mononuclear phagocytic system (MPS) located primarily in the liver and spleen, thereby limiting the dose available for the disease site.[14−16]

Several strategies have been proposed to address this limitation. The primary strategy includes grafting hydrophilic polymers such as polyethylene glycol (PEG) and poloxamer molecules on the nanoparticle surface to decrease MPS uptake.[17,18] PEG serves to mitigate the interactions of nanoparticles with macrophages in the MPS, thereby reducing their immune clearance. However, PEG-modified nanoparticles have been shown to activate the immune system and lose efficacy upon repeated administrations.[19−21] Conjugation of CD47 or peptides derived from this self-recognition determinant to the surface of NP is an alternative approach.[22]

In theory, blood elements with a favorable circulation profile may be used as "natural carriers" improving the NP pharmacokinetics. For example, red blood cells (RBCs) represent an attractive carrier for optimizing NP circulation and, perhaps, delivery to certain intravascular targets.[23−26] Preclinical studies in diverse animal species documented that the coupling of drugs to a RBC surface improves their delivery and therapeutic effects.[27−29] Coupling of NPs to RBCs has the potential to dramatically alter NP behavior in circulation. In addition, pharmacokinetics of

* Address correspondence to samir@engineering.ucsb.edu.

Received for review September 16, 2013 and accepted November 1, 2013.

Published online November 01, 2013
10.1021/nn404853z

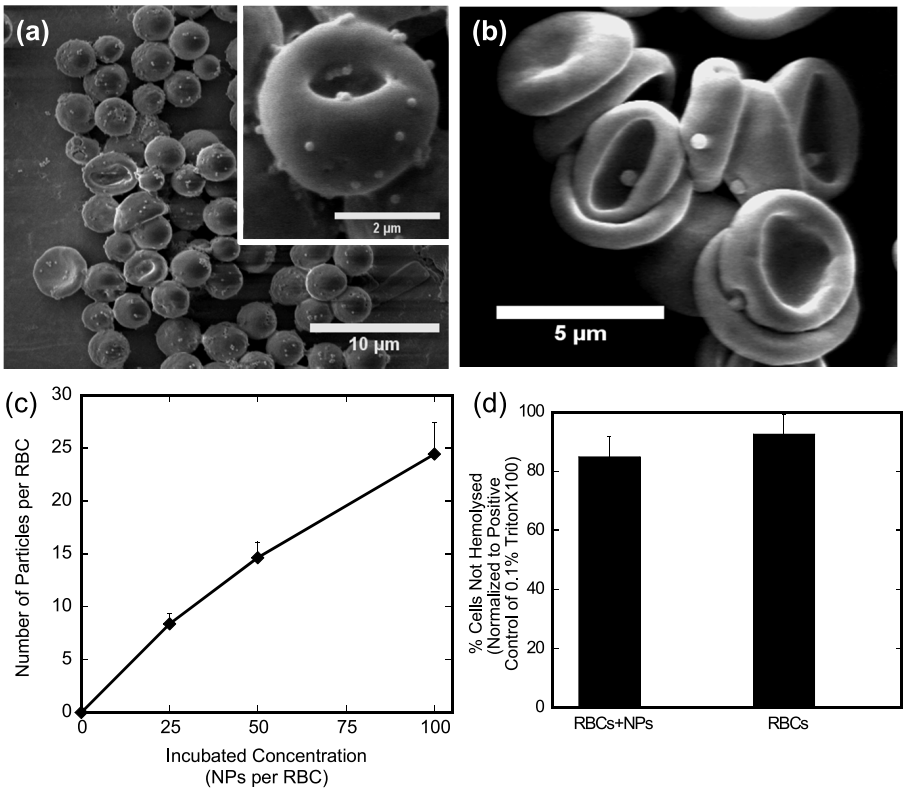

Figure 1. Attachment of nanoparticles to red blood cells (a) Scanning electron micrographs of 200 nm polystyrene spheres attached to RBCs. (b) Scanning electron micrographs of 500 nm polystyrene spheres attached to RBCs. (c) Analysis of RBC-bound 200 nm particles *via* ^{3}H -labeling showing average number of nanoparticles attached per RBC with increasing particle concentration. Values represent mean ± SD (n = 3). (d) RBCs+NPs at high loading (100:1 NP:RBC loading ratio) show no significant lysis compared to RBCs in identical buffer. Data is normalized to a positive control of 1% Triton-X-100. Values represent mean ± SD (n = 3).

the RBC/NP complex may be more favorable than that of free NP in some medical settings. Here, we investigate this hypothesis and demonstrate that attachment to RBCs reduces NP uptake by the MPS organs (liver and spleen).

RESULTS

Attachment of Nanoparticles. Spherical polystyrene nanoparticles (200 nm or 500 nm diameter) were attached to RBCs by incubation at varying particle/RBC ratios up to 100:1. Particle attachment to RBC was mediated by electrostatic and hydrophobic interactions.[23,30,31] The attachment was confirmed through SEM (Figures 1a,b) and was quantified using ^{3}H-radiolabeled nanoparticles (Figure 1c). At a particle/RBC ratio of 100:1, RBCs on average carried ~24 particles (200 nm) per cell (Figure 1c). Under these conditions, >99% of RBCs carried at least 1 attached particle (Supporting Information, Figure 1). Attachment of particles did not induce RBC hemolysis (Figure 1d).

Nanoparticles attached to RBCs did not detach from RBCs under static conditions (Figure 2a). Yet the binding was reversible and particles detached from RBCs upon exposure to physiological shear stresses experienced by RBCs in circulation (5 Pa for 15 min at 37 °C, Figure 2b). In theory, this may enable a natural mechanism for release or transfer of NP load. Microscopic observations of RBCs supported this notion. Nanoparticle-laden RBCs were structurally fixed prior to exposure to shear, and small indentations that matched the size of the particles were found. These indentations likely represent areas where nanoparticles were once attached (Figure 2c). When RBCs were structurally fixed *after* shear-induced particle detachment, no indentations were seen (Figure 2d). The presence of reversible indentations suggests that adhesion of nanoparticles on RBCs is mediated by the spreading of RBC membrane on the surface of hydrophobic nanoparticles. This spreading should increase the RBC-particle contact area, thus leading to a strong adhesion. However, upon shear-induced detachment, RBC's fluid membrane is able to reversibly return to its original shape.

Effect of NP on Circulation of Carrier RBCs. RBCs are the longest circulating cells in the body, circulating up to 120 days in humans. The effect of NP attachment on RBC circulation of RBCs was studied at two doses (low, 10:1, and high, 100:1). Attachment of NPs to RBCs at low doses did not significantly ($p > 0.05$) decrease circulation time of these modified RBCs compared to native RBCs at low dose (Figure 3, open vs hatched bars). The half-lives of RBCs with and without NPs were comparable (33.5 ± 2.1 and 33.6/−5.8 h, respectively). Attachment of NPs at higher doses (100:1) (Figure 3, black bars) however,

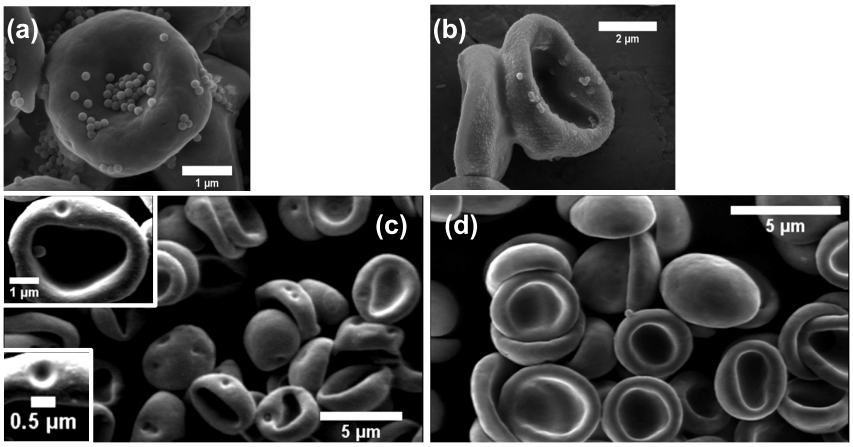

Figure 2. Detachment of nanoparticles from red blood cells Controlled detachment of nanoparticles from RBC surface *via* applied shear stress using a rheometer: (a) no induced shear, and (b) 5 Pa shear stress for 15 min at 37 °C. (c) Scanning electron micrographs of 500 nm polystyrene spheres detached from RBCs *after* fixation with glutaraldehyde showing indents caused by particles attachment and (d) scanning electron micrographs of 500 nm polystyrene spheres detached from RBCs *prior* to fixation with glutaraldehyde showing that indents are reversible and do not permanently deform RBCs.

induced a decrease in circulation of RBCs likely due to accelerated removal of RBCs carrying multiple particles.

Biodistribution of Red Blood Cells. Next, we tested whether NP carriage affects RBC uptake in the organs. RBCs were labeled with ^{51}Cr and their biodistribution was examined for high-loaded RBCs (100:1:NP:RBC incubation). For these experiments, organs were not perfused so as to reveal the potential effect that nanoparticles may have on irreversible uptake and reversible retention of RBCs in the lumen (i.e., hyperemia) in organs. At 1 h (Figure 4a) biodistribution of RBCs with or without NPs was comparable. Similarly, at 24 h, organ retention of RBCs with and without NPs was near the same (Figure 4b). Results in Figure 4 indicate that attachment of NPs to RBCs does not influence organ distribution or retention of RBCs in the spleen, which is known to sequester and clear damaged or irregular RBCs. Some differences were noted in both kidney and liver; however, retention of RBCs in these organs was extremely low and does not significantly contribute to RBC clearance, compared to other organs, in either group.

Biodistribution of Nanoparticles. Carriage by RBCs cardinally changed organ distribution of the nanoparticles. First, the blood level of RBC-NP was ~2−3 times higher than that of free NPs (Supporting Information, Figure 2a) at all time points. Therefore, as expected, RBC carrier markedly prolongs NP circulation. The major difference in blood level between free and RBC-bound NP should be taken into account in assessing their uptake in the organs, for example, to detect nanoparticles that are retained in the tissue *versus* those in the residual blood pool. For this, prior to assessing particle accumulation, organs were perfused to remove blood. After 1 h, nanoparticle uptake in the spleen was reduced by over 50% compared to free particles (Figure 5a: white bars, free nanoparticles; black bars, RBC-adsorbed nanoparticles). More importantly,

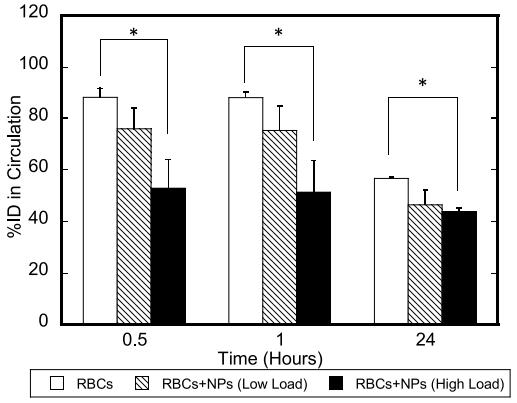

Figure 3. Time-dependent *in vivo* circulation of ^{51}Cr-RBCs. Bar graph representing percentage of injected dose (%ID) for free ^{51}Cr-RBCs (white), ^{51}Cr-RBCs with nanoparticles attached at low loading of 1:10 (hatched), and 1:100 (black) incubation ratios (RBCs/NPs) over a 24 h period. Values represent mean ± SEM (n = 3−6) The asterisk (*) denotes statistical difference from the labeled groups (p < 0.05).

accumulation in lungs was increased ~5-fold. Even after 24 h, nanoparticle persistence in the lungs was still elevated (~3-fold) for RBC-adsorbed nanoparticles compared to free nanoparticles (Figure 5b: white bars, free nanoparticles; black bars, RBC-adsorbed nanoparticles). Enhanced accumulation was also seen in brain, kidneys, intestine, skin, heart, and blood at 1 h (Supporting Information, Figure 2b: white bars, free nanoparticles; black bars, RBC-adsorbed nanoparticles).

Kinetics of Pulmonary Accumulation of RBC-Carried NP. We studied the kinetics of NP biodistribution after administration in the free or RBC-adsorbed form. Free nanoparticles exhibited relatively low accumulation in lungs of about 4%ID/gram (Figure 6a, circles, see Supporting Information Figure 2c for complete NP biodistribution). The majority of the particles were deposited in the liver

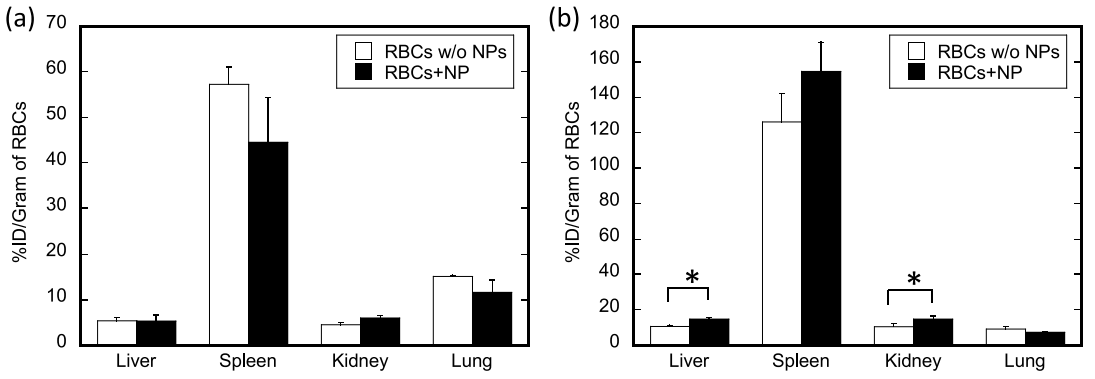

Figure 4. Time-dependent *in vivo* biodistribution of ^{51}Cr-RBCs. Bar graph represents percentage of injected dose per gram of organ tissue (%ID/g) for free ^{51}Cr-RBCs (white), and ^{51}Cr-RBCs with nanoparticles attached (black) at (a) short (1 h) and (b) long (24 h) times. Values represent mean ± SEM (n = 3−6). The asterisk (*) denotes statistical difference from the labeled groups (p < 0.05).

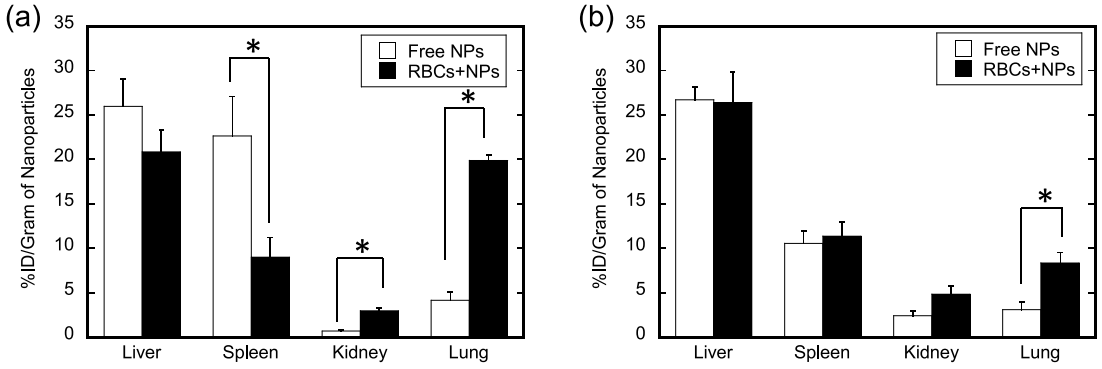

Figure 5. Time-dependent *in vivo* biodistribution of ^{3}H-nanoparticles. Bar graph representing percentage of injected dose per gram of organ tissue (%ID/g) for free ^{3}H-nanoparticles (white), and RBC bound ^{3}H-nanoparticles (black) at (a) short (1 h) and (b) long (24 h) times. Values represent mean ± SEM (n = 3−5). The asterisk (*) denotes statistical difference from the labeled groups (p < 0.05).

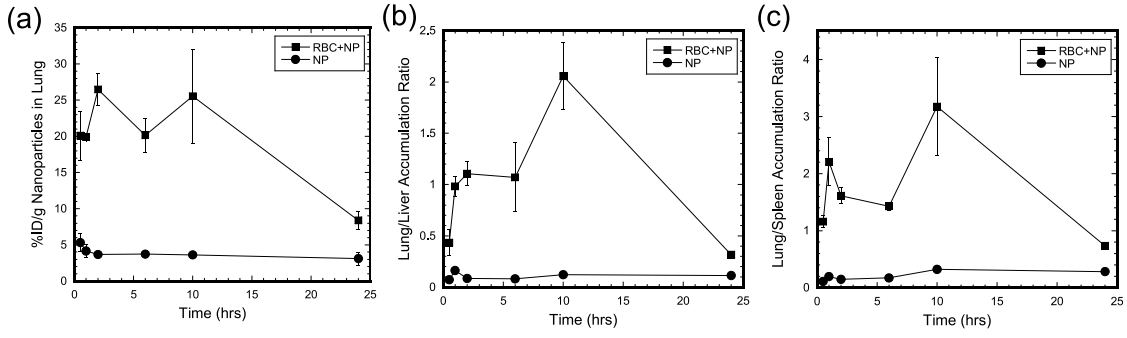

Figure 6. Kinetics of ^{3}H-nanoparticle targeting to lungs while avoiding clearance organs. (a) ^{3}H-Nanoparticle accumulation in lungs represented as percentage of injected dose per gram of lung tissue (%ID/g) for free ^{3}H-nanoparticles (circles), and RBC bound ^{3}H-nanoparticles (squares). (b) Lung to liver ratio of ^{3}H-nanoparticle accumulation represented as percentage of injected dose per gram of organ tissue (%ID/g) for free ^{3}H-nanoparticles (circles), and RBC bound ^{3}H-nanoparticles (squares). (c) Lung to spleen ratio of ^{3}H-nanoparticle accumulation represented as percentage of injected dose per gram of organ tissue (%ID/g) for free ^{3}H-nanoparticles (circles), and RBC bound ^{3}H-nanoparticles (squares). Values represent mean ± SEM (n = 3−5). All RBC+NPs groups were statistically different (p < 0.05) from NP alone groups at all time points for each panel (a,b,c).

and spleen. In contrast, RBC-adsorbed nanoparticles exhibited high lung accumulation within 30 min (Figure 6a, squares, see Supporting Information, Figure 2d for complete RBC+NP biodistribution). The lung accumulation of adsorbed particles was about 5-fold higher compared to that of free particles over a range of 10 h with a maximum enhancement of 7-fold seen at 10 h. Lung accumulation decreased and approached that of free nanoparticles after 24 h (Figure 6a). However, even at 24 h, lung accumulation was significantly higher (p < 0.05) for RBC+NP groups compared to free NPs at all time points. In addition to increasing lung accumulation, RBC-adhesion also decreased liver and spleen clearance of nanoparticles.

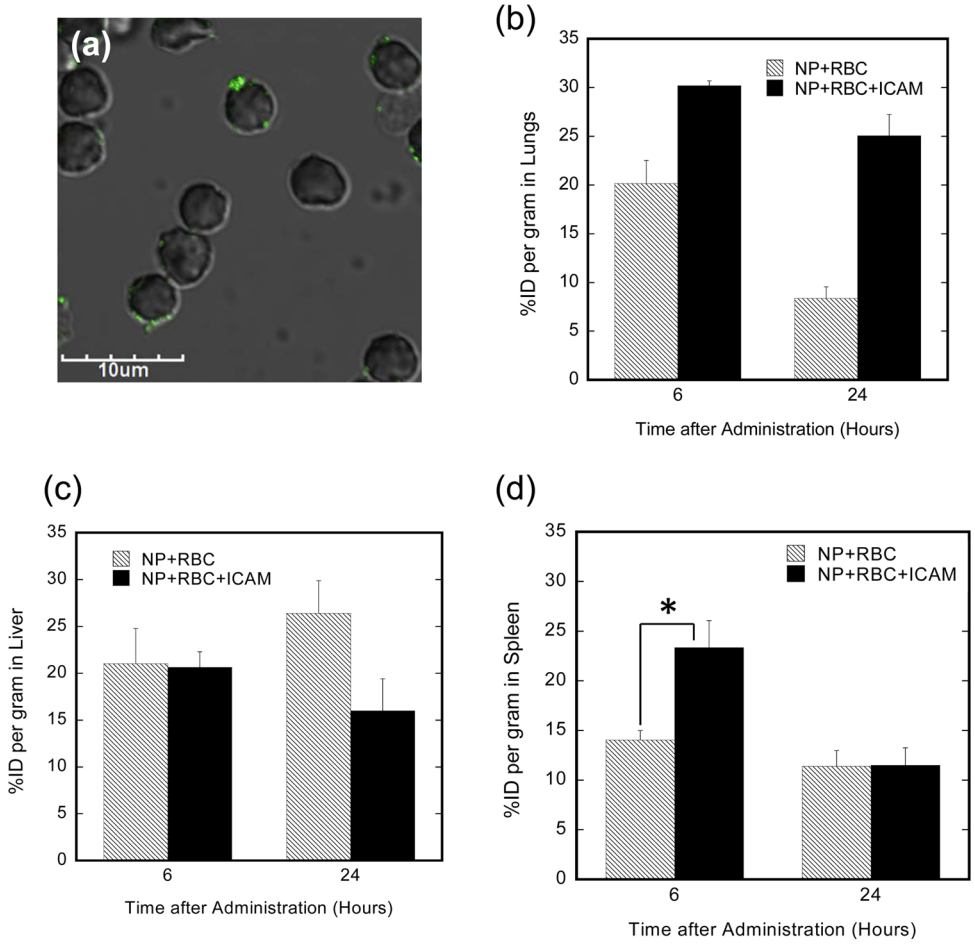

Figure 7. *In vivo* **biodistribution of anti-ICAM-1-coated RBC-bound nanoparticles. (a) Confocal image of fluorescently labeled anti-ICAM-1 binding only to 200 nm PS spheres and not RBC membranes. (b) Lung accumulation (%ID/gram) of RBC/NP (hatched bars) and RBC/NP+anti-ICAM-1 (black bars) complexes at 6 and 24 h. Both lung %ID/gram groups were statistically different ($p < 0.05$). (c) Liver accumulation (%ID/gram) of RBC-NP (hatched bars) and RBC/NP+anti-ICAM-1 (black bars) complexes at 6 and 24 h. (d) Spleen accumulation (%ID/gram) of RBC/NP (hatched bars) and RBC-NP+anti-ICAM-1 (black bars) complexes at 6 and 24 h. The asterisk (*) denotes statistical difference from the labeled groups ($p < 0.05$).**

Collectively, RBC-adhesion led to increased lung/liver accumulation ratio of nanoparticles (Figure 6b, circles *versus* squares) and an increased lung/spleen accumulation ratio of nanoparticles (Figure 6c: circles *versus* squares). Lung/liver and lung/spleen accumulation values of free nanoparticles did not change significantly over a period of 24 h, averaging at about 0.10 for lung/liver and 0.20 for lung/spleen. In contrast, the lung/liver accumulation ratio for RBC-adhered nanoparticles changed significantly over 24 h, peaking at a value of ~2 at 10 h, a value over 15-fold higher than that for free nanoparticles. All lung/liver and lung/spleen ratios were significantly higher ($p < 0.05$) for RBC+NP groups compared to free NPs at all time points, illustrating the ability of hitchhiked nanoparticles to target lungs while avoiding reticulo-endothelial system (RES) organs. Hitchhiking on RBCs also increased accumulation in kidneys and the heart, although the enhancement due to hitchhiking was less prominent than that in lungs. Interestingly, the drop in concentration seen in case of lungs at 24 h was not seen for kidneys or heart (Supporting Information Figure 2d).

Addition of anti-ICAM-1 Antibody. We assessed whether the drop in NP lung accumulation over 24 h (Figure 6a) can be mitigated by adsorption of anti-ICAM-1 antibody (Ab) on the exposed surface of NPs. NPs were first adsorbed to RBCs, and anti-ICAM-1 Ab was then passively adsorbed onto the exposed carboxylated surface of NP ($21.99 \pm 5.15\ \mu$g of ICAM-1 Ab per mg of particle). Confocal microscopy confirmed that anti-ICAM-1 Ab attached only to the NP surface and not to RBC membranes (Figure 7a). Biodistribution was assessed at two points, 6 and 24 h as representative short and long times. Anti-ICAM-1 Ab-coated RBC+NP complexes exhibited increased lung accumulation compared to RBC+NP with no anti-ICAM-1 Ab (Figure 7b). Lung accumulation of NPs for RBC-NP, which otherwise decreased from 6 to 24 h was maintained at a high level by the presence of anti-ICAM-1 Ab. Further, addition of anti-ICAM-1 further decreased liver accumulation of NPs (Figure 7c). However, anti-ICAM-1 conjugation increased spleen retention for RBC+NP complexes at 6 h (Figure 7d), which is expected due to the expression

of anti-ICAM-1 receptor in spleen tissue.[32] Complete biodistribution for anti-ICAM-1-modified RBC+NP complexes was also determined (Supporting Information, Figure 3a,b).

DISCUSSION

The results presented here demonstrate the ability of cellular hitchhiking to reduce MPS clearance and enhance accumulation in lungs. Nanoparticles were reversibly and noncovalently adsorbed on the surface of RBCs. Upon intravenous administration, particles desorbed likely because of shear (Figure 2b) or direct RBC-endothelium contact during their passage through the tissue microvasculature. This desorption occurred rapidly as ~6% of NPs attached to RBCs remained in circulation after 30 min. This is well below the half-life of RBCs themselves (~33 h). In other words, particles detach from RBCs much faster than the rate at which RBCs themselves are removed from circulation. The precise rate of NP detachment and its mechanisms require further assessment. The rate of detachment is likely to depend on the size and geometry of vasculature as well as the location of NP attachment to RBC. It is likely that NPs attached to the outer part of RBC may detach more rapidly than those attached to the central dimple. NP and RBC biodistribution data from Figures 3 and 4 together indicate that there is a transfer of nanoparticles from RBCs to endothelium in the vasculature. Transient accumulation of detached NPs in lungs (Figure 6a) suggests that NPs that are not bound to endothelium or internalized are likely washed away by the blood over 24 h. This is also evident from the effect of anti-ICAM-1 Ab on the retention of NPs in the vasculature. The presence of anti-ICAM-1 Ab is likely to increase binding strength of NPs to the endothelium[33] as well as lead to increased internalization, both of which will increase the persistence of NPs in endothelium. A schematic (Figure 8) provides a hypothesis how NPs detach from RBCs in microcirculation. On the basis of the large amount of NPs present in lungs when adsorbed onto RBCs, their detachment from the RBCs is attributed to the squeezing of RBC through tiny capillaries smaller in diameter than the RBC itself, which are present in air−blood-barrier microcirculation.[34] Pulmonary vasculature contains ~25−30% of the total endothelial surface in the body and receives the entire venous cardiac output for oxygenation *via* pulmonary arterial trunk, in addition to a fraction of arterial cardiac output *via* intercostal and pleural vessels.[35] This high percentage of endothelium that receives >50% of total cardiac blood output combined with forced RBC-endothelial contact in the lung vasculature is proposed to facilitate detachment of NPs from RBCs and subsequent accumulation in lungs. Uptake in the lung is unlikely to be mediated by macrophages. While some mammalian species have macrophages active in endothelium, this is typically not the case for healthy rodents.[36−38] Further, the lung macrophages

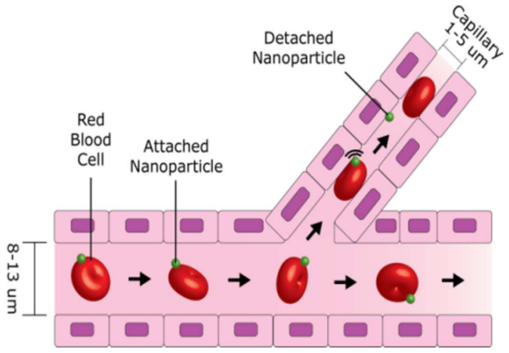

Figure 8. Schematic of particle detachment from RBCs in small capillaries. Schematic representing the detachment of NPs from RBCs in tiny capillaries present in lung microvasculature.

are present on the air side of the vasculature; hence the NPs will make first contact with endothelial cells and not macrophages.

RBC-hitchhiking thus provides a natural means to deliver nanoparticles in the close vicinity of vascular endothelium in lungs. The beneficial effects of RBC-adhesion mediated NP delivery are expected to be higher in tissues with extensive microvascular networks as is the case for lungs. Mouse lung capillaries possess an average diameter of 5 μm reaching sizes as small as 1 μm, 3−4 times smaller than RBC diameters to enable their close contact with the endothelium so as to facilitate oxygen transport. The close contact likely plays a role in dislodging the nanoparticles.

RBC-bound NPs circulate for much longer and in higher percentages than freely administered NPs. Circulation and organ distribution of RBCs themselves was not impaired due to NP attachment. To ensure that the ^{3}H-NP signal was due to NPs and not blood remaining in organs, organs were perfused for all NP-tracing experiments. This ensures that the measured NP biodistribution corresponds to NPs that have either detached from RBCs and bind to endothelium or have been internalized by the endothelium. On the other hand, for ^{51}Cr-RBC tracing experiments, organs were not perfused so as to examine the effect NP attachment had on RBC biodistribution. Circulation and biodistribution of independently traced RBC-bound ^{3}H-labeled-NPs and ^{51}Cr-labeled-RBCs indicate a true transfer of NPs from RBCs to endothelium. Dislodged nanoparticles remain in tissues either due to nonspecific interactions with the endothelium or due to internalization by the cells. Persistence of nanoparticle accumulation in tissues was found to depend on the tissue type and was extended, in the case of lungs, by conjugation of the anti-ICAM-1 Ab to the NP surface for RBC/NP complexes. For RBC/NP complexes, enhanced accumulation persisted in heart and kidneys for a period of 24 h, the accumulation peaked at 10 h for lungs followed by a substantial decline by 24 h. However, after conjugation with anti-ICAM-1, %ID/gram in lungs and persistence in the lungs at 24 h was significantly

increased (Figure 7b). Nanoparticles were able to avoid the liver and spleen over a period of 24 h when attached to RBCs. Liver and spleen are known to rapidly remove all foreign entities from the blood, and developing nanoparticle therapies which both target other organs while avoiding liver and spleen has been a challenge.[39]

Adhesion of nanoparticles did not produce adverse effects on RBCs. No significant impact of nanoparticle adhesion on the morphology or function of RBCs was seen. No hemolysis of RBCs due to nanoparticle adhesion was observed. The only change seen in the membrane morphology was directly underneath the membrane, which appeared to be induced by spreading the RBC membrane on the particle surface. However, this change was reversible. Physically damaged cells are generally removed from the circulation predominately by the spleen[40] and to a less extent by the liver;[41] therefore it is imperative that RBC morphology not be significantly altered as RBCs must perform their natural functions when nanoparticles are attached. Further, since no statistical difference in RBC accumulation for either unmodified RBCs or NP-loaded RBCs was noted in the spleen at any time point, it is not expected that NP modification of RBCs is affecting clearance in this major RBC clearance organ. Previous studies have shown that while nanoparticles are ultimately removed from the circulation, RBCs which once carried nanoparticles continue to remain in circulation.[23] Further, the fraction of total RBCs in circulation that were labeled by nanoparticles in these experiments was small (1.7%). Hence, the likelihood of nanoparticles-laden RBCs significantly impacting overall circulation is negligible.

Simultaneously, NP conjugation to RBCs enhances the accumulation of NPs in highly vascularized organs, first of all, as lungs. Because of the extended surface area and privileged perfusion by >50% of the total cardiac blood output, pulmonary endothelium represents a preferential target,[42] in particular, for antibodies to endothelial surface determinants including anti-ICAM-1.[43,44] In this vein, by conjugating anti-ICAM-1 to RBC/NP complexes, the persistence of NPs targeted to lung can be maintained over a period of 24 h while RBC/NP lung persistence, without anti-ICAM-1 modification, is limited to much shorter times.

At a fundamental level, the use of RBC-adsorbed NPs provides a new hybrid approach for drug delivery. Synthetic systems such as polymeric nanoparticles offer the advantages of control over particle composition and manufacturability; however, they suffer from the limitation of immune clearance. RBCs, on the other hand, naturally avoid RES clearance for four months and continuously reach all tissues. An approach based on the use of synthetic nanoparticles to encapsulate drugs and deliver them to tissues using RBCs offers an optimal blend of natural and synthetic systems. RBC-adsorption also provides an ideal blend of enhanced circulation and targeting. Currents means of enhancing circulation are based on the use of PEG or polaxamers, which suffer from limited circulation times and accelerated clearance after repeat injections.[21,45,46] The ability of RBC-hitchhiking NPs to exhibit longer circulation and tissue deposition after repeat injections needs further investigations. Several additional questions need to be answered before full potential of RBC-mediated NP delivery can be realized. These include understanding the fate of NPs in organs, limits of NP loading on RBCs, and behavior of NPs after repeat injections. It should also be noted that this method requires the use of a patient's own blood cells or the use of any other RBCs that can be transfused into patients.

Hitchhiking onto mammalian cells is also observed in nature by certain pathogens such as *Mycoplasma hemofelis* (previously known as hemobartonella), which remain circulating inside mammals by hitchhiking on the surface of RBCs.[47] Recently, hitchhiking onto the surface of mammalian cells has received attention as a new approach of drug delivery. Specifically, RBCs have been used to prolong *in vivo* circulation of nanoparticles.[23,24] The results reported here build on these findings and demonstrate tissue accumulation of nanoparticles. In addition, T cells have also been used for cellular hitchhiking, where drug loaded liposomes were conjugated directly to the T cell surface for efficient elimination of EG7-OVA and EL4 tumors.[48] Additional systems are also being developed on the basis of specific cell surface receptors present on B cells, monocytes, and macrophages for attachment of drug carrying backpacks.[49,50]

Cellular-hitchhiking provides a novel means to address two major issues that nanoparticle therapies routinely face; the avoidance of MPS organs, liver and spleen, and targeted delivery to difficult-to-reach sites in the body such as brain and lungs. While studies reported here were performed with nonbiodegradable polystyrene particles, RBC hitchhiking can be extended to biodegradable PLGA nanoparticles (Supporting Information, Figure 4). With further research focused on understanding the mechanisms of particle detachment from RBCs and their interactions with the endothelium, RBC-hitchhiking nanoparticles may open new opportunities on therapeutic delivery.

METHODS

Blood Collection and Storage. Whole blood was collected from healthy female BALB/c mice (18−20 g; 8−10 weeks old). Mice were sacrificed by CO_2 overdose and blood was collected *via* cardiac puncture and stored in heparin-coated tubes. Blood was stored at 4 °C for no longer than 2 days for all experiments. Blood was resuspended in 4% sodium citrate (pH 7.4). Whole blood was centrifuged at room temperature at 100 g and supernatant was discarded leaving purified red blood cells.

Particle Preparation. Fluorescently and nonfluorescently labeled carboxylated polystyrene (PS) particles (200 nm) were

purchased from Polysciences. Particles were radiolabeled with tritium (^{3}H) conjugated oleic acid (Moravek Biochemicals). Briefly, 20% w/v PS particles in water were added to a solution containing 100 μL of ^{3}H-oleic acid, 100 μL of ethanol, and 25 μL of tetrahydrofuran for 30 min with constant rotation. Particles were then washed 10 times *via* centrifugation for 30 min at 15000*g* to remove unincorporated oleic acid.

PLGA nanoparticles were prepared *via* standard nanoprecipitation techniques: briefly, an organic phase with 75 mg of PLGA polymer in 7.5 mL of acetone opposite an aqueous 2% poly vinyl alcohol solution. The organic phase was added dropwise to the aqueous phase using a syringe pump at 15 mL/h with continuous stirring (300 rpm). PLGA nanoparticles were purified *via* centrifugation and characterized using TEM.

Attachment of Nanoparticles to RBCs. Nanoparticles and RBCs were suspended in 4% sodium citrate. A known number of nanoparticles were incubated with RBCs at room temperature for 30 min. Unbound nanoparticles were separated from RBCs with bound nanoparticles *via* centrifugation. *anti*-ICAM-1 Ab was added to RBC-nanoparticle conjugates at a concentration of 400 μg/mL in PBS for 1 h under constant rotation. The detachment of particles performed under shear was performed using an AR-G2 rheometer from TA Instruments. Particle-RBC conjugates were resuspended in plasma proteins and serum prior to detachment in order to prevent reattachment of nanoparticles. Particle-RBC conjugates were exposed to 5 Pa of shear stress for 15 min at 37 °C. Detachment was visually confirmed using a scanning electron microscope (see below).

Fluorescence-Activated Cell Sorting (FACS). Nanoparticles, red blood cells and conjugates were suspended in PBS. A FACSAria Flow Cytometer with a 70 μm nozzle was used to quantify attachment of nanoparticles to red blood cells. Mammalian cells were filtered prior to analysis of the sample. BD FACSDiva software 6.0 was used to analyze data.

Scanning Electron Microscopy (SEM). An FEI XL40 SEM at 3−5 kV with a 5 mm working distance was used for imaging both cells and particles. Images were taken after 2 min of palladium coating (at 10 kV) *via* a Hummer sputtering system. Cells were imaged in a dehydrated state and prepared using a standard cell surface fixation technique. Briefly, cell samples were incubated with a 2.5% glutaraldehyde solution for the cross-linking of surface proteins. This provides cells with the required stability that live tissue samples do not possess, which is necessary while imaging under high voltage and vacuum.

Transmission Electron Microscopy (TEM). An FEI T20 was used to characterize PLGA nanoparticles. A 2 μL sample of diluted PLGA nanoparticles was deposited on a copper grid and dried in air prior to imaging.

Confocal Microscopy. An Olympus Fluoview 500 (Olympus America Inc. Center Valley, PA, USA) was used to image fluorescently labeled anti-ICAM-1 Ab modified NPs attached to RBCs.

Tissue Distribution and Blood Clearance of RBC/NPs in Mice. ^{51}Cr-labeled mouse RBCs (^{51}Cr-RBC) were prepared as described[51] and ^{51}Cr-RBC/NP groups were prepared as discussed earlier. Naive BALB/c female mice (18−20 g; n = 3−6 per group) were anesthetized and injected intravenously *via* the jugular vein with approximately 10 μCi of ^{51}Cr-RBC or ^{51}Cr-RBC/NP formulations. At designated time points postinjection, blood was collected from the retro-orbital sinus and organs (kidneys, liver, spleen, and lung) were collected and weighed. Blood samples were withdrawn in heparin tubes, centrifuged at 1200*g*, and the radioactivity in plasma, RBC pellets, and organs was measured in a gamma-counter.

***In Vivo* Biodistribution.** For nanoparticle biodistribution studies, 5×10^9 radiolabeled particles in Alsever's buffer were injected *via* tail vein into healthy female BALB/c mice (18−20 g; n = 3−5 per group). At predetermined time points, the mice were anesthetized and euthanized by opening the chest cavity and perfusion of PBS through the left ventricle. Known weights of liver, spleen, kidney, heart, lungs, brain, intestine, skin, and blood were harvested and dissolved overnight in Solvable (Perkin-Elmer). The following morning, liquid scintillation counting efficiency cocktail Ultima Gold (Perkin-Elmer) was added to organ solutions and organs were measured for their radioactive content in a Packard TriCarb 2100TR scintillation counter. All animal protocols were approved by respective Institutional Animal Care and Use Committees (IACUC) at the University of California, Santa Barbara and University of Pennsylvania.

Conflict of Interest: The authors declare no competing financial interest.

Acknowledgment. A.C.A. was supported by the National Science Foundation Graduate Research Fellowship under Grant No. DGE-1144085. The MRL Central Facilities are supported by the MRSEC Program of the NSF under Award No. DMR 1121053; a member of the NSF-funded Materials Research Facilities Network (www.mrfn.org). This study was supported in part by NIH *via* grants to V.R.M. (HL087036, HL090697 and HL121134). The authors would like to thank P. Cheng and M. Helgeson of UCSB for rheometer use and training.

Supporting Information Available: Additional figures as described in the text. This material is available free of charge *via* the Internet at http://pubs.acs.org.

REFERENCES AND NOTES

1. Azarmi, S.; Roa, W. H.; Lobenberg, R. Targeted Delivery of Nanoparticles for the Treatment of Lung Diseases. *Adv. Drug Delivery Rev.* **2008**, *60*, 863–875.
2. Faraji, A. H.; Wipf, P. Nanoparticles in Cellular Drug Delivery. *Bioorg. Med. Chem.* **2009**, *17*, 2950–2962.
3. Wang, A. Z.; Langer, R.; Farokhzad, O. C. Nanoparticle Delivery of Cancer Drugs. *Annu. Rev. Med.* **2012**, *63*, 185–198.
4. Dhar, S.; Gu, F. X.; Langer, R.; Farokhzad, O. C.; Lippard, S. J. Targeted Delivery of Cisplatin to Prostate Cancer Cells by Aptamer Functionalized Pt(Iv) Prodrug-PLGA-PEG Nanoparticles. *Proc. Natl. Acad. Sci. U.S.A.* **2008**, *105*, 17356–17361.
5. Peer, D.; Karp, J. M.; Hong, S.; Farokhzad, O. C.; Margalit, R.; Langer, R. Nanocarriers as an Emerging Platform for Cancer Therapy. *Nat. Nanotechnol.* **2007**, *2*, 751–760.
6. Brannon-Peppas, L.; Blanchette, J. O. Nanoparticle and Targeted Systems for Cancer Therapy. *Adv. Drug Delivery Rev.* **2004**, *56*, 1649–1659.
7. Davis, M. E.; Chen, Z. G.; Shin, D. M. Nanoparticle Therapeutics: An Emerging Treatment Modality for Cancer. *Nat. Rev. Drug Discovery* **2008**, *7*, 771–782.
8. Hrkach, J.; Von Hoff, D.; Mukkaram Ali, M.; Andrianova, E.; Auer, J.; Campbell, T.; De Witt, D.; Figa, M.; Figueiredo, M.; Horhota, A.; *et al.* Preclinical Development and Clinical Translation of a Psma-Targeted Docetaxel Nanoparticle with a Differentiated Pharmacological Profile. *Sci. Transl. Med.* **2012**, *4*, 128ra39.
9. Kattan, J.; Droz, J. P.; Couvreur, P.; Marino, J. P.; Boutan-Laroze, A.; Rougier, P.; Brault, P.; Vranckx, H.; Grognet, J. M.; Morge, X.; *et al.* Phase I Clinical Trial and Pharmacokinetic Evaluation of Doxorubicin Carried by Polyisohexylcyanoacrylate Nanoparticles. *Invest. New Drugs* **1992**, *10*, 191–199.
10. Green, M. R.; Manikhas, G. M.; Orlov, S.; Afanasyev, B.; Makhson, A. M.; Bhar, P.; Hawkins, M. J. Abraxane, a Novel Cremophor-Free, Albumin-Bound Particle Form of Paclitaxel for the Treatment of Advanced Non-Small-Cell Lung Cancer. *Ann. Oncol.* **2006**, *17*, 1263–1268.
11. Hofheinz, R. D.; Gnad-Vogt, S. U.; Beyer, U.; Hochhaus, A. Liposomal Encapsulated Anti-Cancer Drugs. *Anticancer Drugs* **2005**, *16*, 691–707.
12. Allen, T. M.; Cullis, P. R. Drug Delivery Systems: Entering the Mainstream. *Science* **2004**, *303*, 1818–1822.
13. Ruoslahti, E. Peptides as Targeting Elements and Tissue Penetration Devices for Nanoparticles. *Adv. Mater.* **2012**, *24*, 3747–3756.
14. Yoo, J. W.; Chambers, E.; Mitragotri, S. Factors That Control the Circulation Time of Nanoparticles in Blood: Challenges, Solutions and Future Prospects. *Curr. Pharm. Des.* **2010**, *16*, 2298–2307.
15. Riehemann, K.; Schneider, S. W.; Luger, T. A.; Godin, B.; Ferrari, M.; Fuchs, H. Nanomedicine--Challenge and Perspectives. *Angew. Chem., Int. Ed. Engl.* **2009**, *48*, 872–897.

16. Sanhai, W. R.; Sakamoto, J. H.; Canady, R.; Ferrari, M. Seven Challenges for Nanomedicine. *Nat. Nanotechnol.* **2008**, *3*, 242–244.
17. Perry, J. L.; Reuter, K. G.; Kai, M. P.; Herlihy, K. P.; Jones, S. W.; Luft, J. C.; Napier, M.; Bear, J. E.; DeSimone, J. M. PEGylated Print Nanoparticles: The Impact of Peg Density on Protein Binding, Macrophage Association, Biodistribution, and Pharmacokinetics. *Nano Lett.* **2012**, *12*, 5304–5310.
18. Bazile, D.; Prud'homme, C.; Bassoullet, M. T.; Marlard, M.; Spenlehauer, G.; Veillard, M. Stealth Me.PEG-PLA Nanoparticles Avoid Uptake by the Mononuclear Phagocytes System. *J. Pharm. Sci.* **1995**, *84*, 493–498.
19. Ishida, T.; Maeda, R.; Ichihara, M.; Irimura, K.; Kiwada, H. Accelerated Clearance of PEGylated Liposomes in Rats after Repeated Injections. *J. Controlled Release* **2003**, *88*, 35–42.
20. Ishida, T.; Masuda, K.; Ichikawa, T.; Ichihara, M.; Irimura, K.; Kiwada, H. Accelerated Clearance of a Second Injection of PEGylated Liposomes in Mice. *Int. J. Pharm.* **2003**, *255*, 167–174.
21. Ishida, T.; Ichihara, M.; Wang, X.; Yamamoto, K.; Kimura, J.; Majima, E.; Kiwada, H. Injection of PEGylated Liposomes in Rats Elicits PEF-Specific IgM, Which Is Responsible for Rapid Elimination of a Second Dose of Pegylated Liposomes. *J. Controlled Release* **2006**, *112*, 15–25.
22. Rodriguez, P. L.; Harada, T.; Christian, D. A.; Pantano, D. A.; Tsai, R. K.; Discher, D. E. Minimal "Self" Peptides That Inhibit Phagocytic Clearance and Enhance Delivery of Nanoparticles. *Science* **2013**, *339*, 971–975.
23. Chambers, E.; Mitragotri, S. Prolonged Circulation of Large Polymeric Nanoparticles by Non-Covalent Adsorption on Erythrocytes. *J. Controlled Release* **2004**, *100*, 111–119.
24. Chambers, E.; Mitragotri, S. Long Circulating Nanoparticles Via Adhesion on Red Blood Cells: Mechanism and Extended Circulation. *Exp. Biol. Med. (Maywood, NJ, U.S.)* **2007**, *232*, 958–966.
25. Muzykantov, V. R.; Sakharov, D. V.; Smirnov, M. D.; Domogatsky, S. P.; Samokhin, G. P. Targeting of Enzyme Immobilized on Erythrocyte Membrane to Collagen-Coated Surface. *FEBS Lett.* **1985**, *182*, 62–66.
26. Muzykantov, V. R. Drug Delivery by Red Blood Cells: Vascular Carriers Designed by Mother Nature. *Exper. Opin. Drug Delivery* **2010**, *7*, 403–427.
27. Muzykantov, V. R.; Sakharov, D. V.; Smirnov, M. D.; Samokhin, G. P.; Smirnov, V. N. Immunotargeting of Erythrocyte-Bound Streptokinase Provides Local Lysis of a Fibrin Clot. *Biochim. Biophys. Acta* **1986**, *884*, 355–362.
28. Zaitsev, S.; Spitzer, D.; Murciano, J. C.; Ding, B. S.; Tliba, S.; Kowalska, M. A.; Marcos-Contreras, O. A.; Kuo, A.; Stepanova, V.; Atkinson, J. P.; *et al.* Sustained Thromboprophylaxis Mediated by an RBC-Targeted Pro-Urokinase Zymogen Activated at the Site of Clot Formation. *Blood* **2010**, *115*, 5241–5248.
29. Danielyan, K.; Ganguly, K.; Ding, B. S.; Atochin, D.; Zaitsev, S.; Murciano, J. C.; Huang, P. L.; Kasner, S. E.; Cines, D. B.; Muzykantov, V. R. Cerebrovascular Thromboprophylaxis in Mice by Erythrocyte-Coupled Tissue-Type Plasminogen Activator. *Circulation* **2008**, *118*, 1442–1449.
30. Yoon, J.-Y.; Kim, J.-H.; Kim, W.-S. Interpretation of Protein Adsorption Phenomena onto Functional Microspheres. *Colloids Surf., B* **1998**, *12*, 15–22.
31. Yoon, J.-Y.; Park, H.-Y.; Kim, J.-H.; Kim, W.-S. Adsorption of BSA on Highly Carboxylated Microspheres—Quantitative Effects of Surface Functional Groups and Interaction Forces. *J. Colloid Interface Sci.* **1996**, *177*, 613–620.
32. Hayes, S. H.; Seigel, G. M. Immunoreactivity of ICAM-1 in Human Tumors, Metastases and Normal Tissues. *Int. J. Clin. Exp. Pathol.* **2009**, *2*, 553.
33. Kolhar, P.; Anselmo, A. C.; Gupta, V.; Pant, K.; Prabhakarpandian, B.; Ruoslahti, E.; Mitragotri, S. Using Shape Effects to Target Antibody-Coated Nanoparticles to Lung and Brain Endothelium. *Proc. Natl. Acad. Sci. U.S.A.* **2013**, *110*, 10753–10758.
34. Sikora, L.; Johansson, A. C.; Rao, S. P.; Hughes, G. K.; Broide, D. H.; Sriramarao, P. A Murine Model to Study Leukocyte Rolling and Intravascular Trafficking in Lung Microvessels. *Am. J. Pathol.* **2003**, *162*, 2019–2028.
35. Fishman, A. Dynamics of the Pulmonary Circulation. *Handb. Physiol.* **1963**, *2*, 1667–1743.
36. Brain, J. D.; Molina, R. M.; DeCamp, M. M.; Warner, A. E. Pulmonary Intravascular Macrophages: Their Contribution to the Mononuclear Phagocyte System in 13 Species. *Am. J. Physiol.: Lung Cell. Mol. Physiol.* **1999**, *276*, L146–L154.
37. Warner, A.; Barry, B.; Brain, J. Pulmonary Intravascular Macrophages in Sheep: Morphology and Function of a Novel Constituent of the Mononuclear Phagocyte System. *Lab. Invest.* **1986**, *55*, 276–288.
38. Warner, A. E.; Brain, J. D. Intravascular Pulmonary Macrophages: A Novel Cell Removes Particles from Blood. *Am. J. Physiol.* **1986**, *250*, R728–732.
39. Moghimi, S. M.; Hunter, A. C.; Murray, J. C. Long-Circulating and Target-Specific Nanoparticles: Theory to Practice. *Pharmacol. Rev.* **2001**, *53*, 283–318.
40. Crosby, W. H. Normal Functions of the Spleen Relative to Red Blood Cells: A Review. *Blood* **1959**, *14*, 399–408.
41. Terpstra, V.; van Berkel, T. J. Scavenger Receptors on Liver Kupffer Cells Mediate the *in Vivo* Uptake of Oxidatively Damaged Red Blood Cells in Mice. *Blood* **2000**, *95*, 2157–63.
42. Muzykantov, V. R. Biomedical Aspects of Targeted Delivery of Drugs to Pulmonary Endothelium. *Exper. Opin. Drug Delivery* **2005**, *2*, 909–926.
43. Muro, S.; Garnacho, C.; Champion, J. A.; Leferovich, J.; Gajewski, C.; Schuchman, E. H.; Mitragotri, S.; Muzykantov, V. R. Control of Endothelial Targeting and Intracellular Delivery of Therapeutic Enzymes by Modulating the Size and Shape of ICAM-1-Targeted Carriers. *Mol. Ther.* **2008**, *16*, 1450–1458.
44. Scherpereel, A.; Wiewrodt, R.; Christofidou-Solomidou, M.; Gervais, R.; Murciano, J. C.; Albelda, S. M.; Muzykantov, V. R. Cell-Selective Intracellular Delivery of a Foreign Enzyme to Endothelium *in Vivo* Using Vascular Immunotargeting. *FASEB J.* **2001**, *15*, 416–426.
45. Ishihara, T.; Takeda, M.; Sakamoto, H.; Kimoto, A.; Kobayashi, C.; Takasaki, N.; Yuki, K.; Tanaka, K.; Takenaga, M.; Igarashi, R.; et al. Accelerated Blood Clearance Phenomenon Upon Repeated Injection of Peg-Modified Pla-Nanoparticles. *Pharm. Res.* **2009**, *26*, 2270–2279.
46. Ishida, T.; Harada, M.; Wang, X. Y.; Ichihara, M.; Irimura, K.; Kiwada, H. Accelerated Blood Clearance of Pegylated Liposomes Following Preceding Liposome Injection: Effects of Lipid Dose and Peg Surface-Density and Chain Length of the First-Dose Liposomes. *J. Controlled Release* **2005**, *105*, 305–317.
47. Criado-Fornelio, A.; Martinez-Marcos, A.; Buling-Sarana, A.; Barba-Carretero, J. C. Presence of Mycoplasma Haemofelis, Mycoplasma Haemominutum and Piroplasmids in Cats from Southern Europe: A Molecular Study. *Vet. Microbiol.* **2003**, *93*, 307–317.
48. Stephan, M. T.; Moon, J. J.; Um, S. H.; Bershteyn, A.; Irvine, D. J. Therapeutic Cell Engineering with Surface-Conjugated Synthetic Nanoparticles. *Nat. Med.* **2010**, *16*, 1035–1041.
49. Doshi, N.; Swiston, A. J.; Gilbert, J. B.; Alcaraz, M. L.; Cohen, R. E.; Rubner, M. F.; Mitragotri, S. Cell-Based Drug Delivery Devices Using Phagocytosis-Resistant Backpacks. *Adv. Mater.* **2011**, *23*, H105–109.
50. Swiston, A. J.; Gilbert, J. B.; Irvine, D. J.; Cohen, R. E.; Rubner, M. F. Freely Suspended Cellular "Backpacks" Lead to Cell Aggregate Self-Assembly. *Biomacromolecules* **2010**, *11*, 1826–1832.
51. Muzykantov, V. R.; Seregina, N.; Smirnov, M. D. Fast Lysis by Complement and Uptake by Liver of Avidin-Carrying Biotinylated Erythrocytes. *Int. J. Artif. Organs* **1992**, *15*, 622–627.